ISSN 1674-1056
http://cpb.iphy.ac.cn
http://iopscience.iop.org/cpb
中国物理 B
Chinese Physics
中国物理 Chinese Physics B

Robust two-gap strong coupling superconductivity associated with low-lying phonon modes in pressurized Nb_5Ir_3O superconductors

Bosen Wang(王铂森)[1,2,4], Yaoqing Zhang(张尧卿)[3], Shuxiang Xu(徐淑香)[1], Kento Ishigaki[2], Kazuyuki Matsubayashi[2], Jin-Guang Cheng(程金光)[1,4], Hideo Hosono[3], Yoshiya Uwatoko[2]

Citation: Chin. Phys. B . 2019, 28(10): 107401 . **doi:** 10.1088/1674-1056/ab4047
Journal homepage: http://cpb.iphy.ac.cn; http://iopscience.iop.org/cpb

What follows is a list of articles you may be interested in

Crystal structures and sign reversal Hall resistivities in iron-based superconductors $Li_x(C_3H_{10}N_2)_{0.32}FeSe$ ($0.15 < x < 0.4$)

Rui-Jin Sun(孙瑞锦), Shi-Feng Jin(金士锋), Jun Deng(邓俊), Mu-Nan Hao(郝木难), Lin-Lin Zhao(赵琳琳), Xiao Fan(范晓), Xiao-Ning Sun(孙晓宁), Jian-Gang Guo(郭建刚), Lin Gu(谷林)

Chin. Phys. B . 2019, 28(6): 067401 . **doi:** 10.1088/1674-1056/28/6/067401

Electronic structure and nematic phase transition in superconducting multiple-layer FeSe films grown by pulsed laser deposition method

Bing Shen(沈兵), Zhong-Pei Feng(冯中沛), Jian-Wei Huang(黄建伟), Yong Hu(胡勇), Qiang Gao(高强), Cong Li(李聪), Yu Xu(徐煜), Guo-Dong Liu(刘国东), Li Yu(俞理), Lin Zhao(赵林), Kui Jin(金魁), X J Zhou(周兴江)

Chin. Phys. B . 2017, 26(7): 077402 . **doi:** 10.1088/1674-1056/26/7/077402

Electronic structure of transition metal dichalcogenides $PdTe_2$ and $Cu_{0.05}PdTe_2$ superconductors obtained by angle-resolved photoemission spectroscopy

Liu Yan, Zhao Jian-Zhou, Yu Li, Lin Cheng-Tian, Hu Cheng, Liu De-Fa, Peng Ying-Ying, Xie Zhuo-Jin, He Jun-Feng, Chen Chao-Yu, Feng Ya, Yi He-Mian, Liu Xu, Zhao Lin, He Shao-Long, Liu Guo-Dong, Dong Xiao-Li, Zhang Jun, Chen Chuang-Tian, Xu Zu-Yan, Weng Hong-Ming, Dai Xi, Fang Zhong, Zhou Xing-Jiang

Chin. Phys. B . 2015, 24(6): 067401 . **doi:** 10.1088/1674-1056/24/6/067401

Magnetic phase transitions and large mass enhancement in single crystal $CaFe_4As_3$

Zhang Xiao-Dong, Wu Wei, Zheng Ping, Wang Nan-Lin, Luo Jian-Lin

Chin. Phys. B . 2012, 21(1): 017402 . **doi:** 10.1088/1674-1056/21/1/017402

RAPID COMMUNICATION

Robust two-gap strong coupling superconductivity associated with low-lying phonon modes in pressurized Nb_5Ir_3O superconductors*

Bosen Wang(王铂森)[1,2,4,†], Yaoqing Zhang(张尧卿)[3], Shuxiang Xu(徐淑香)[1], Kento Ishigaki[2], Kazuyuki Matsubayashi[2], Jin-Guang Cheng(程金光)[1,4], Hideo Hosono[3], and Yoshiya Uwatoko[2]

[1] *Beijing National Laboratory for Condensed Matter Physics and Institute of Physics, Chinese Academy of Sciences, Beijing* 100190, *China*
[2] *Institute for Solid State Physics, University of Tokyo, Kashiwanoha* 5-1-5, *Kashiwa, Chiba* 277-8581, *Japan*
[3] *Materials Research Center for Element Strategy, Tokyo Institute of Technology, Yokohama* 226-8503, *Japan*
[4] *Songshan Lake Materials Laboratory, Dongguan* 523808, *China*

(Received 16 June 2019; revised manuscript received 15 August 2019; published online 30 September 2019)

We report robust superconducting state and gap symmetry of Nb_5Ir_3O via electrical transport and specific heat measurements. The analysis of specific heat manifests that Nb_5Ir_3O is a strongly coupled superconductor with $\Delta C/\gamma_n T_c \sim 1.91$ and double s-wave superconducting gaps of $2\Delta_L(0)/k_B T_c \sim 6.56$ and $2\Delta_S(0)/k_B T_c \sim 2.36$ accounting for 90% and 10%, respectively. The $(C_p - \gamma_n T)/T^3$ vs. T plot shows a broad peak at ~ 23 K, indicating phonon softening and the appearance of low-lying phonon mode associated with the interstitial oxygen. This behavior explains the monotonic increase of T_c in $Nb_5Ir_3O_{(1-\delta)}$ by strengthening the electron–phonon coupling and enlarging the density of states at Fermi level. The Hall coefficient is temperature independent below 200 K, and changes its sign from positive to negative above 250 K, suggesting that carrier is across the hole- to electron-dominant regions and the multi-band electronic structures. On warming, the resistivity shows a gradual crossover from T^2- to T^3-dependence at a critical temperature T^*, and a broad peak at a temperature T_p. The reduced T_c under pressure is linearly correlated with lattice parameters c/a ratio and T_p, suggesting the important phonon contributions in Nb_5Ir_3O as a phonon-medicated superconductor. Possible physical mechanisms are proposed.

Keywords: new superconductor, high-pressure effect, strongly coupled superconductor

PACS: 74.70.–b, 74.62.Fj **DOI:** 10.1088/1674-1056/ab4047

Low energy anharmonic lattice vibration significantly affects electron–phonon coupling (λ_{e-p}) and plays an important role in exploring superconductors (SC) and revealing superconducting mechanism.[1,2] Among them, phonon softening associated with structural instabilities usually results in Fermi surface nesting and the enhancement of the electron–phonon coupling, which is believed to be much important for superconducting pairings.[3–7] Various cage-like materials have been reported and attracted much more attention.[3,6,7] The commonalities are composed of hollow covalently bonded atomic clusters and various inserted elements, offering playgrounds to explore diverse structures, exotic physics, and multifunctionalities, e.g., multi-band SCs,[3,8–10] metal–insulator transition,[10] thermoelectricity,[11] and electrides.[12,13] But some regularity is not universal concerning the superconducting pairing mechanisms, which is also challenging to study these scientific issues.

Hexagonal structure Mn_5Si_3-type derivatives are such examples.[14,15] One of the top priorities is the explorations of new SCs and superconducting mechanisms.[15–19] At present, the difficulty in synthesizing single-phase hexagonal and tetragonal materials lies in their close formation energies.[16,17,19] One common way is elementary intercalation into interstitial positions of $Mn_5Si_3M_x$ (M = carbon, nitrogen, oxide, and transition metal elements, etc).[14–19] Hexagonal phase can be stabilized and the relevant studies are performed to reveal the relationships between lattice instabilities and superconductivity. For example, hexagonal Nb_5Ir_3 is stabilized upon the insertion of the interstitial oxygen and T_c is increased as a result. It is sure that the interstitial oxygen brings great changes in electronic structures.[16] It still remains unclear whether the enhanced T_c is dominantly associated to the volume change, band fillings, structural instability, and/or disorders.[16] Another issue to be addressed is the relationship of electride and superconductivity. Theoretical calculations predicated that the electride nature of Nb_5Ir_3 vanishes in Nb_5Ir_3O. As we know, eletride materials have electronic bands of anionic electron near Fermi level (E_F) in many cases including C12A7: e-1 electride, Ca_2N, and Y_5Si_3, which is the important reason why electride ma-

*Project supported by the National Key Research and Development Program of China (Grant Nos. 2018YFA0305700 and 2018YFA0305800), JSPS Kakenhi (Grant No. 17H06153), the Strategic Priority Research Program and Key Research Program of Frontier Sciences of the Chinese Academy of Sciences (Grant Nos. XDB25000000 and QYZDB-SSW-SLH013), the National Natural Science Foundation of China (Grant No. 11574377), Beijing Natural Science Foundation, China (Grant No. Z190008), IOP Hundred-Talent Program, China (Grant No. Y7K5031 × 61), and the Youth Promotion Association, Chinese Academy of Sciences (Grant No. 2018010).

†Corresponding author. E-mail: bswang@iphy.ac.cn

© 2019 Chinese Physical Society and IOP Publishing Ltd

terials exhibit interesting properties. For SCs, T_c is enhanced along with the suppression of the electride nature and the coexistence of superconductivity and electride is firstly reported with $T_c \sim 0.16$–2.4 K.[12,13] For C12A7: e-1 electride SC, T_c is increased to 2.4 K by pressure and this enhancement is attributed to the changes in electronic nature of anionic electride band crossing Fermi levels switching from s- to sd-hybridized state.[13] However, the interstitial oxygen suppresses superconducting state in other cases, hexagonal Zr_5Sb_3 is superconductive at ~ 2.3 K, but Zr_5Sb_3O is not superconducting above 1.8 K, it is thought that larger density of states (DOS) at E_F associated with the Zr-d electrons and the larger value of λ_{e-p} is critical.[15] Analogously, in $Zr_5Sb_{(3-x)}Ru_x$, its hexagonal structure transforms into W_5Si_3-type one for $0.4 \leq x \leq 0.6$.

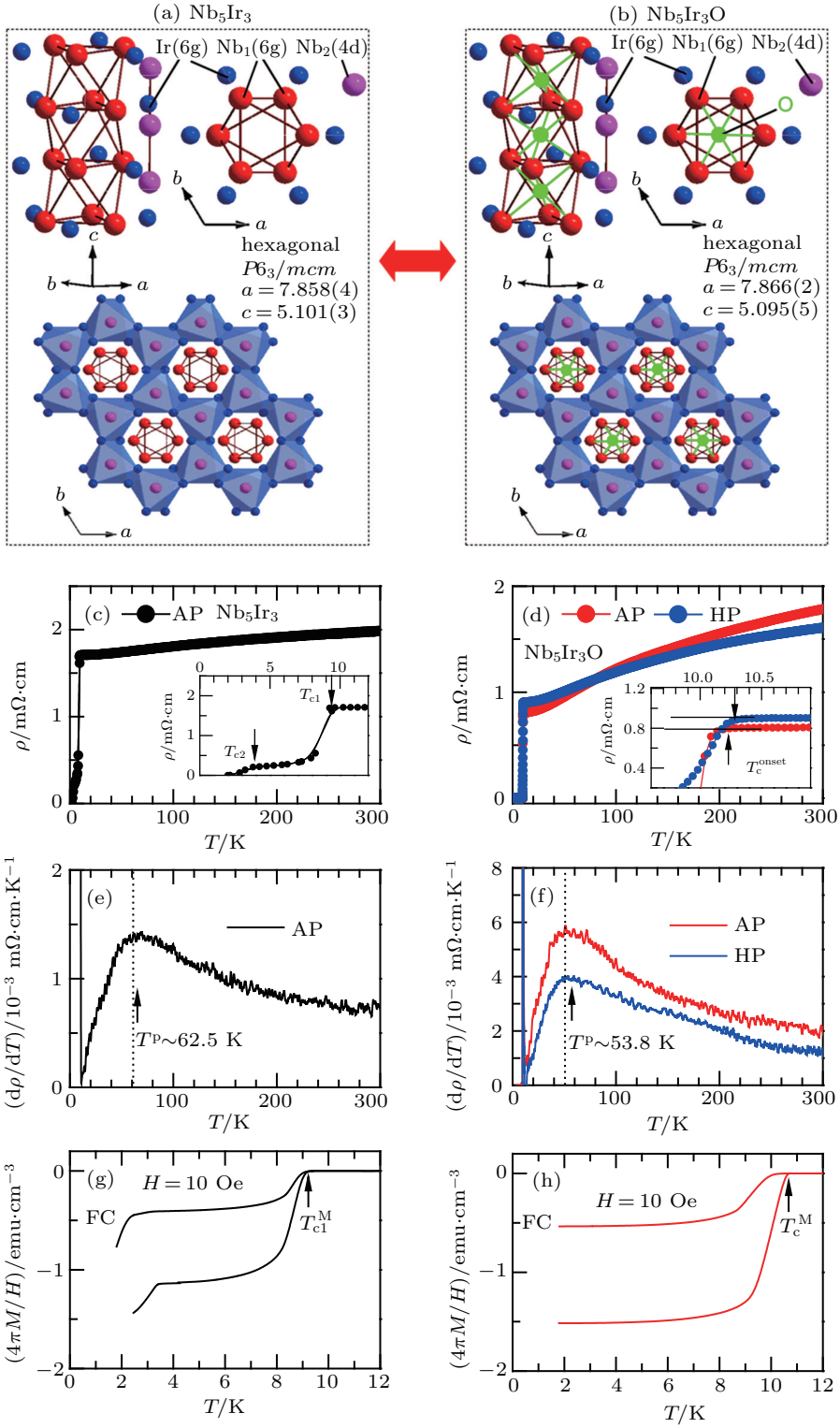


Fig. 1. Crystal structures for (a) Nb_5Ir_3 and (b) Nb_5Ir_3O. $\rho(T)$ for (c) Nb_5Ir_3 and (d) Nb_5Ir_3O. The enlargement of low-T data is shown in the inset. The derivative $d\rho/dT$ for (e) Nb_5Ir_3 and (f) Nb_5Ir_3O. The broad peaks are marked by T^p. $M(T)$ curves at 10 Oe under the ZFC and FC processes for (g) Nb_5Ir_3 and (h) Nb_5Ir_3O.

T_c increases from 2.3 K to 5 K in $Zr_5Sb_{2.4}Ru_{0.6}$, which originates from the E_F close to the DOS peak.[17] Except for these above scientific issues, the present studies on the intercalated Mn_5Si_3-type materials focus on macro-correlations of crystal structure and superconductivity, and some conclusions are inadequate. In this work, Nb_5Ir_3O is selected to study the issues further. Another concern is to reveal superconductivity by comparative analysis of doping and high pressure, and to judge whether unconventional or not with magnetism of localized and/or itinerant iridium.[20,21]

High pressure is an effective and clean way to study structural chemistry and electronic phase transitions of materials by shortening bonds and reconstructing electronic bands. For SCs, high-pressure effect is valuable because the underlying mechanism can be identified by analogizing with the known SCs. In this work, Nb_5Ir_3O is found to be a strongly coupled SC with two s-wave gaps and phonon softening associated with interstitial oxygen is critical.

At ambient pressure (AP), electrical transport and specific heat of Nb_5Ir_3 and Nb_5Ir_3O were measured on commercial physical properties measurement system (PPMS, 1.8 K $\leq T \leq$ 300 K, -9 T $\leq H \leq$ 9 T). High-pressure susceptibility was measured in a piston-cylinder cell with glycerol as the pressure transmitting medium (PTM) and a small piece lead as the pressure monitor. The background contributions mainly originate from Meissner signal of Pb reference. High-pressure electrical transport was performed by the four-probe method in a cubic anvil pressure cell which generated the hydrostatic environment.[22] MgO cubes were used as the gasket and glycerol as PTM. All the measurements were carried out in ^{4}He refrigerated chambers (1.9 K $\leq T \leq$ 300 K).

Structures of Nb_5Ir_3 and $Nb_5Ir_3O_{(1-\delta)}$ are shown in Figs. 1(a) and 1(b). They have similar hexgonal symmetry except for the interstitial oxygen inserted. Nb_5Ir_3 contains two groups of weakly connected octahedra along the c axis: one is hollow $(Nb1)_6$ octahedron connected by Nb1–Nb1 bonds, the other is side-sharing $Ir(Nb2)_6$ octahedron. Moreover, it is regarded as the network of twisted trigonal Nb1-prisms connected by the planes along the c axis, which allows the insertion of oxide ion in the "Nb1 cages". It does not change the crystal structure, but forms covalent bonds Nb1–O. Upon changing from Nb_5Ir_3 to Nb_5Ir_3O, lattice parameter c contracts by $\sim 0.11\%$ while a and b expand by $\sim 0.087\%$. In Figs. 1(c) and 1(d), $\rho(T)$ of Nb_5Ir_3 and Nb_5Ir_3O shows the metallic behavior. Two independent drops appear in the inset of Fig. 1(c), which represent superconducting transitions of hexagonal and tetragonal Nb_5Ir_3, respectively.[20,21] T_c^{onset} and T_c^{zero} are marked where $\rho(T)$ deviates linearly and is zero. At AP, T_c^{onset} is ~ 9.4 K for hexagonal Nb_5Ir_3 and ~ 4.0 K for tetragonal Nb_5Ir_3, T_c^{onset} is ~ 10.15 K and $T_c^{zero} \sim$ is 10 K for Nb_5Ir_3O. In Fig. 1(d), $\rho(T)$ is shown and similar in temperature dependence for both as-grown Nb_5Ir_3O and annealed one (4 GPa, 600 °C). A clear difference is that high pressure broadens the transition and T_c^{zero} decreases from ~ 10 K to ~ 9.6 K. A broad peak appears in $d\rho/dT$ at a critical temperature T^p, which decreases from ~ 62.5 K to ~ 53.8 K upon the increase of the interstitial oxygen. Usually, this peak reflects the information of the phonon spectrum and is closely related with Debye temperature θ_D.[23]

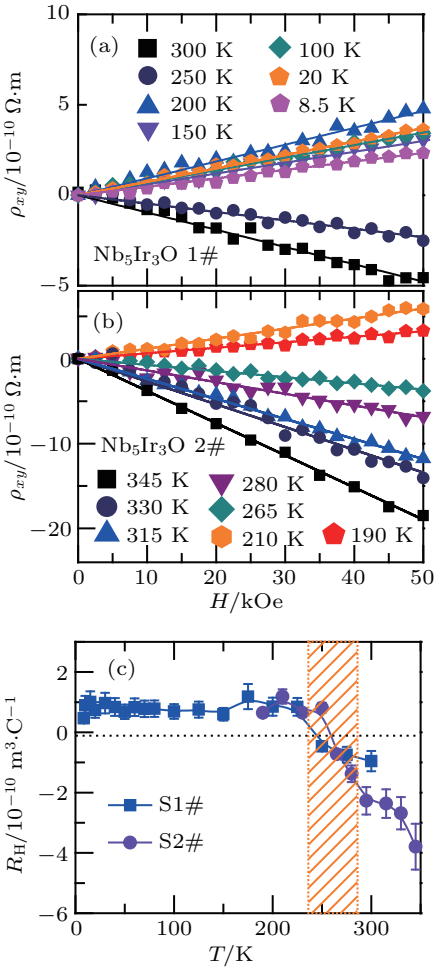


Fig. 2. The transverse resistivity ρ_{xy} vs. H at various temperatures: (a) S1# and (b) S2#. (c) Temperature dependence of Hall coefficient $R_H(T)$.

Figure 2 displays the field-dependence of transverse resistivity ρ_{xy} at various temperatures up to 5 T. ρ_{xy} shows a linear H-dependence for each temperature. Hall coefficient R_H is defined by $d\rho_{xy}/dH$. R_H is positive and almost temperature independent below 200 K, and negative above 250 K, which suggests the balance of electron- to hole-types carriers with different effective masses and velocities. Its strong temperature dependence elucidates that Nb_5Ir_3O has a complex multi-band electronic structure with both electron- and hole-Fermi pockets.[24,25] According to the successive changes in mangetism and electrical resistivity, we can exclude the possible structural and magnetic phase transitions. Besides, the longitudinal resistivity ρ_{xx} is measured, the magnetoresistance $MR = \Delta\rho_{xx}/\rho_{xx}(0) = (\rho_{xx}(5\text{ T}) - \rho_{xx}(0))/\rho_{xx}(0) < 2\%$. As

we know, for a multi-band structure material, it is difficult to calculate the carrier concentration by a single-band model. It is necessary to consider the mobility of two carriers and the specific Fermi surface structures and more theoretical calculations and in-depth experimental analysis are needed. Meanwhile, the carrier density by the simple estimate of the single-band model is only a lower limit of the total carrier number (electrons plus holes), such as $n \sim 1.6 \times 10^{28}$ m^{-3} for Nb_5Ir_3O at 300 K. Considering the change of sign of R_H, the compensation effect at 300 K (where the one-band carrier density was calculated) is expected to still be significant. Further understandings need De-Haas–van Alphen and angle-resolved photoemission spectroscopy.

Temperature dependence of specific heat $C_p(T)$ is shown in Fig. 3(a). On warming, $C_p(T)$ increases and approximates $3NR$ above 300 K. T_c ($\sim$ 9.94 K) is marked by the jump in C_p/T. The inset shows $C_p(T)/T$ and its polynomial fittings $C_p/T = \gamma_n + \beta_1 T^2 + \beta_2 T^4$ in the temperature range of $T_c \le T \le 14$ K, where $\gamma_n T$ and $\beta_1 T^3 + \beta_2 T^5$ are electron and phonon contributions, respectively. It gives γ_n = 34.255 mJ/mol·K^2, β_1 = 0.4489 mJ/mol·K^4, $\beta_2 = 1.07 \times 10^{-3}$ mJ/mol·K^6. Electronic contribution $C_e(T)$ was investigated by the deduction of $\beta_1 T^3 + \beta_2 T^5$ from $C_p(T)$ as in Fig. 3(c). The $\Delta C/\gamma_n T_c$ at T_c is $\sim$ 1.91, larger than 1.43 for a Bardeen–Cooper–Schrieffer (BCS) SC.[26] λ_{e-p} is 0.85 by using McMillan formula $T_c = (\theta_D/1.45)\exp\{-1.04(1+\lambda_{e-p})/[\lambda_{e-p} - 0.15(1+0.62\lambda_{e-p})]\}$, which implies strong electron–phonon coupling.[26]

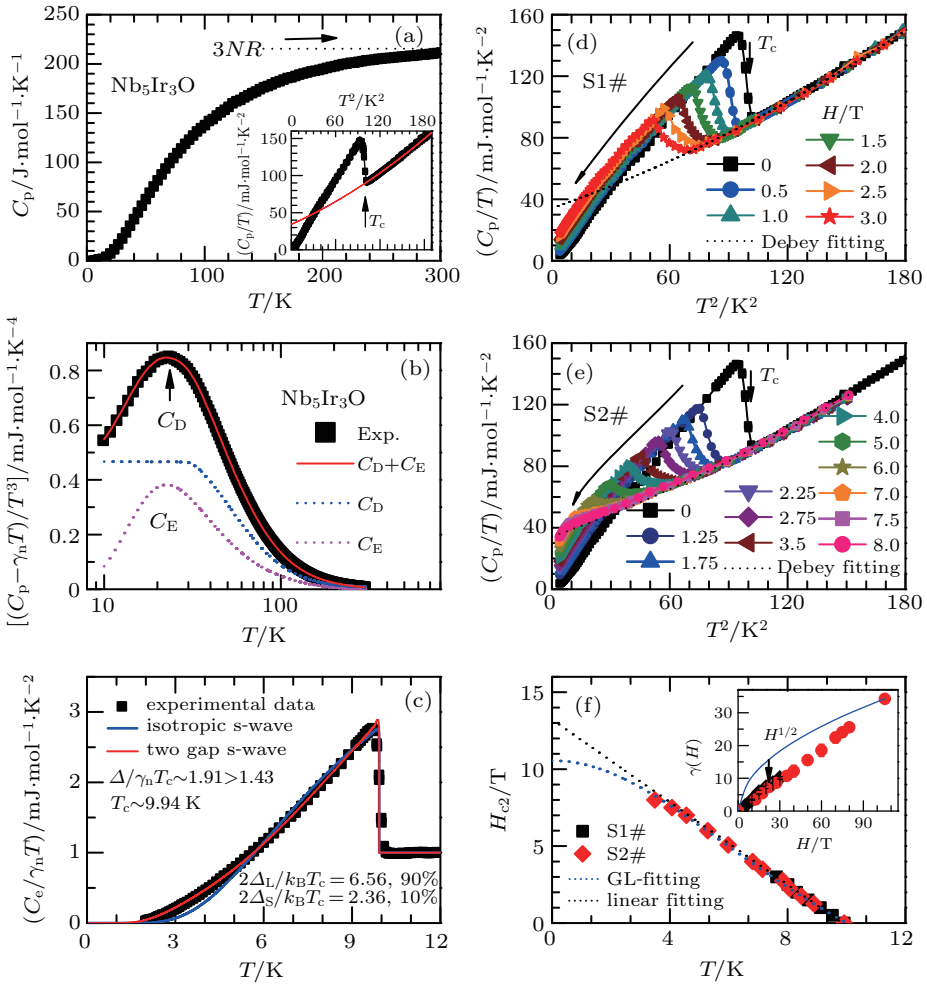


Fig. 3. (a) Temperature dependent $C_p(T)$ for Nb_5Ir_3O, the inset shows low-T $C_p(T)/T$. (b) The $(C_p - \gamma_n T)/T^3$ is the sum of Debye model C_D and Einstein oscillators C_E. (c) Electronic specific heat $C_e(T) = C_p(T) - (\beta_1 T^3 + \beta_2 T^5)$ is analyzed by using a single-gap model as $C_e(T)/T = \beta_1 T^3 + \beta_2 T^5 + B\exp(-\Delta/k_B T)$. (d) and (e) H-dependence of $C_p(T)$. (f) The upper critical field H_{c2} is given by $H_{c2}(T) = H_{c2}(0)[1-(T/T_c)^2]/[1+(T/T_c)^2]$ and $H_{c2}(0) = -0.693 T_c \, dH_{c2}/dT$, respectively. Inset shows H-dependent $\gamma(H)$ and its comparison to $H^{1/2}$-behavior for d-wave SCs.

To get more information on gap symmetry, $C_e(T)$ was analyzed by a single-gap model $C(T) = \beta_1 T^3 + \beta_2 T^5 + B\exp(-\Delta/k_B T)$ at first, which gives $2\Delta/k_B T_c = 4.25$. But clear deviations between experimental and mathematical fitting exist for $T < 5$ K, which implies that isotropic s-wave is too simple. Meanwhile, an anisotropic s-wave gap is similar but not applicable to the present case. Then, two anisotropic s-waves with gaps Δ_1 and Δ_2 are required. The data are well duplicated with $2\Delta_L(0)/k_B T_c \sim 6.56$ (90%) and $2\Delta_S(0)/k_B T_c \sim 2.36$ (10%). Furthermore, H-dependence of $C_e(T,H)$ is measured. At $H = 0$, the linear extrapolation of C_e/T vs. T^2 gives a "residual" Sommerfeld coefficient

$\gamma_0 \approx 0$ mJ·mol^{-1}·K^{-2}. For each H, $\gamma(H)$ at $T = 0$ K is determined by linear fitting to C_e/T vs. T^2. The H-dependence of $\gamma(H)$ is plotted in Fig. 3(f). $\gamma(H)$ increases linearly as a function of H, implying the appearance of nodeless gap. $\gamma(H)$ is smaller than the $H^{1/2}$ dependence for d-wave SCs with line nodes.[27] Generally, in fully-gapped SCs, the excited state is seen as normal-state quasiparticles in vortex core states, which generates the $\gamma_n(H) \approx H$ at zero temperature. Thus, Nb_5Ir_3O is a fully-gapped s-waves SC. Moreover, using the H-dependence of $C_p(T)$ data in Figs. 3(d) and 3(e), the upper critical field $H_{c2}(0)$ is 10.5(5) T and 9.5(8) T by Ginzburg–Landau equation $H_{c2}(T) = H_{c2}(0)[1-(T/T_c)^2]/[1+(T/T_c)^2]$ and Werthamer–Helfand–Hohenberg (WHH) formula $H_{c2}(0) = -0.693 T_c \, dH_{c2}/dT$, respectively.[28]

To extract phonon contributions, the $(C_p - \gamma_n T)/T^3$ vs. T is plotted. It shows a broad peak at ~ 23 K, which manifests the existence of low-energy Einstein vibration associated with anomalies in the phonon spectrum.[29] $C_p(T)$ is the sum of Debye mode and Einstein oscillators

$$C_p(T) - \gamma_n T = C_D(T) + C_E(T), \tag{1}$$

$$C_D(T) = 9NR\left(\frac{T}{\theta_D}\right)^3 \int_0^{\theta_D/T} \frac{\delta^4 e^\delta}{(e^\delta - 1)^2} d\delta, \tag{2}$$

$$C_E(T) = 3N_1R\left(\frac{\theta_{E1}}{T}\right)^2 \frac{\exp\left(\frac{\theta_{E1}}{T}\right)}{\left(\exp\left(\frac{\theta_{E1}}{T}\right)-1\right)^2} + 3N_2R\left(\frac{\theta_{E2}}{T}\right)^2 \frac{\exp\left(\frac{\theta_{E2}}{T}\right)}{\left(\exp\left(\frac{\theta_{E2}}{T}\right)-1\right)^2}, \tag{3}$$

where $C_D(T)$ and $C_E(T)$ are the contributions of continuous phonon mode and localized oscillators, respectively, N, N_1, and N_2 are the numbers of oscillators per formula, R is the gas constant, θ_D and θ_{E1}, θ_{E2} are Debye and Einstein temperatures, respectively. It gives $\theta_D = 315.8(4)$ K, $\theta_{E1} = 87.9(2)$ K, $\theta_{E2} = 69.7(5)$ K, which are insensitive to the temperature ranges selected. As above, the Nb_1O octahedron is connected with side-sharing $Ir(Nb_2)_6$ one, which reminds us that T_c depends on λ_{e-p} in materials with low-lying phonon modes. It suggests the existence of phonon softening associated with interstitial oxygen.

Figure 4 shows $\rho(T)$ of Nb_5Ir_3O under various pressures. With increasing pressure, room-temperature ρ decreases and its value at 13 GPa is nearly three times smaller than that at AP. $\rho(T)$ has similar temperature dependence for each pressure: metallic behavior and entering into superconducting state. As shown in Fig. 4(b), with increasing pressure, T_c^{onset} and T_c^{zero} decrease and transition width ΔT $(= T_c^{onset} - T_c^{zero})$ increases, implying that the superconducting transition is broadened by pressure. As shown in Fig. 4(c), susceptibility is measured in a piston pressure cell. T_c^M is determined by the intersections of two straight lines. Large field shielding effect below T_c^M confirms bulk superconductivity. The fraction is nearly 1 by subtracting the background contributions of Pb signal which is about 5%–10% of total magnetization. T_c^M decreases from ~ 9.91 K at 0.10 GPa to ~ 9.70 K at 1.21 GPa. The stress effect and the enhanced anisotropy by pressure are the main reasons. Besides, the broad peak at $T^p \sim 53.8$ K atAP enhances to 69.4 K at 13 GPa, which is negatively correlated with T_c.

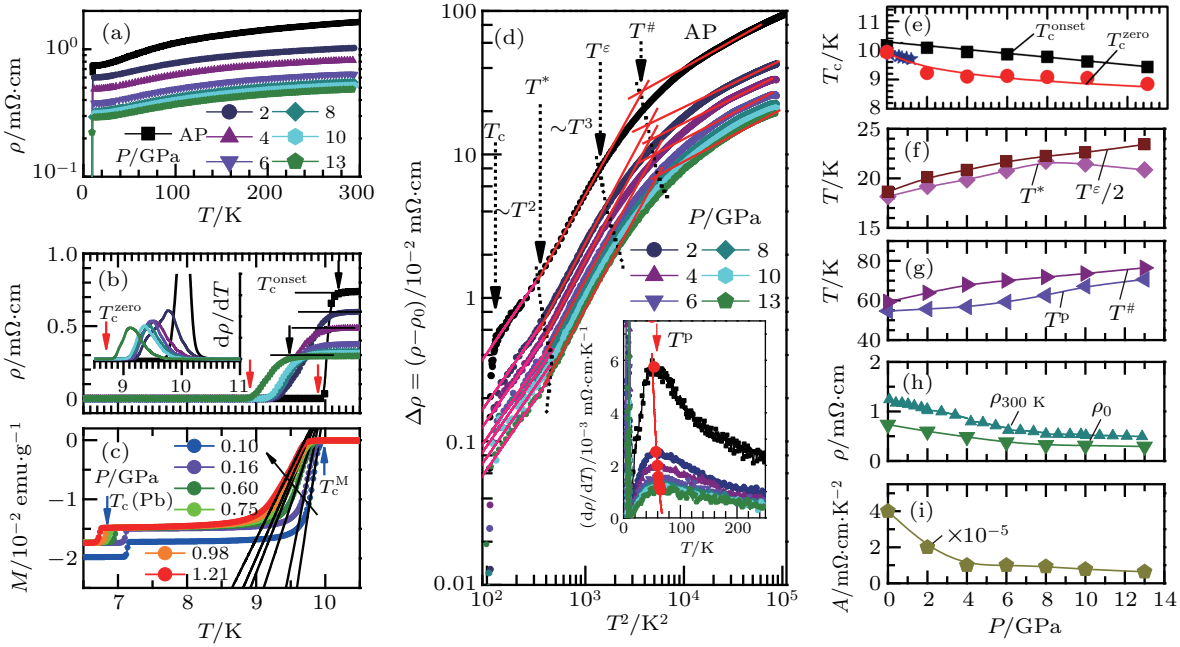


Fig. 4. (a) The $\rho(T)$ under various pressures. (b) Low-T $\rho(T)$ is enlarged and $d\rho/T$ in the inset. (c) $M(T)$ under ZFC process at 10 Oe. (d) $\Delta\rho(T)$ under various pressures and the characteristic temperatures T^*, T^ε, and $T^\#$ are defined as the crossing points from T^2- to T^3-dependence, the deviation from T^3-dependence, the intersection of T^3-dependence and linear fitting, respectively. The parameters are summarized with pressures: (e) T_c^{onset}, T_c^{zero}, (f) T^*, $T^\varepsilon/2$, (g) T^p, $T^\#$, (h) $\rho_{300\,K}$, ρ_0, (i) the A value.

Normal-state $\rho(T)$ is analyzed by $\rho = \rho_0 + AT^n$ with residual resistivity ρ_0, temperature coefficient A, and exponent n. It is found that n is $\sim 2.\pm 0.1$ for $T \leq T^*$, then increases up to $\sim 3.\pm 0.1$ for $T^* \leq T \leq T^\varepsilon$, and then tends to saturation for $T \geq T^\#$, where T^*, T^ε, and $T^\#$ are defined as the crossing points of T^2- to T^3-dependence, the deviation from T^3-dependence, the intersection of T^3-dependence and linear fitting above 250 K, respectively. All the parameters are shown in Figs. 4(f) and 4(g). Considering the small pressure difference and distribution (< 0.5 GPa) in the cubic anvil cell cooling from 300 K to 2 K, the present analyses of temperature dependence of resistivity are reliable. T^ε, $T^\#$, T^p increases as the pressure increases while T^* reaches the maximum at 8 GPa. T^2-fittings for $T_\mathrm{c} \leq T \leq T^*$ give ρ, A and their pressure dependence in Figs. 4(h) and 4(i). Both ρ and $\rho_{300\ \mathrm{K}}$ reduce with increasing pressure. The decrease of ρ is attributed to the weakened grain boundary scatterings under pressure. The A has a positive correlation with T_c: it decreases quickly below 4 GPa, and then trends to a constant.

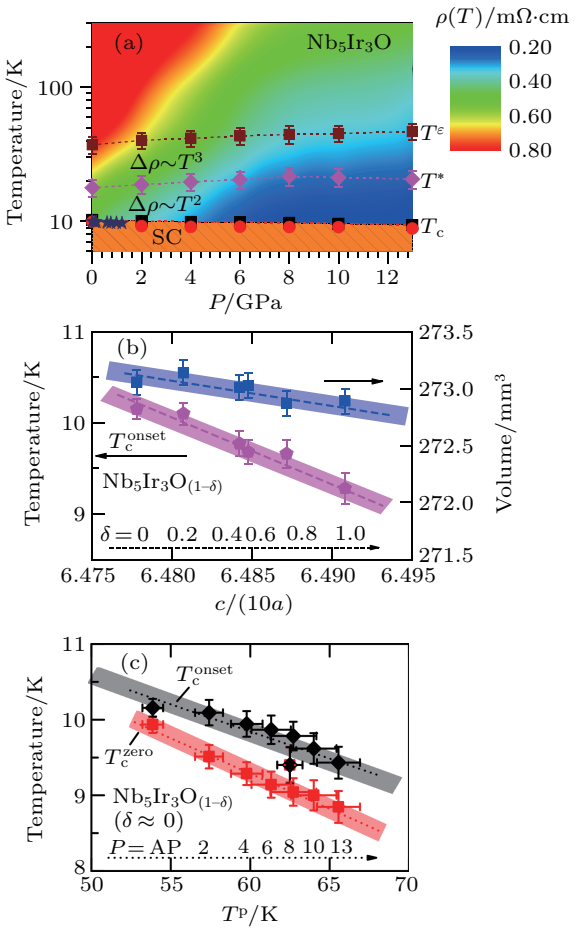


Fig. 5. (a) Pressure phase diagram, the color represents the changing trends of resistivity. (b) The $T_\mathrm{c}^\mathrm{onset}$, the unit-cell volume V, and the lattice parameter ratio $c/(10a)$ are related with the increasing nominal oxide content $(1-\delta)$ of 0, 0.20, 0.40, 0.60, 0.80, 1.0 for $Nb_5Ir_3O_{(1-\delta)}$. (c) We scaled the relationship of $T_\mathrm{c}^\mathrm{onset}$ ($T_\mathrm{c}^\mathrm{zero}$) and T^p for Nb_5Ir_3O. The thick lines indicate the tendency.

In Fig. 5(a), we outline the high-pressure phase diagram. The color represents the changing trend of resistivity. Generally, T^2-dependence for $T_\mathrm{c} \leq T \leq T^*$ shows that electron–electron scattering is the main source and T^3-dependence for $T^* \leq T \leq T^\varepsilon$ indicates important electron–phonon scattering. Above T^ε, $\rho(T)$ is saturated, indicating that electron–phonon scattering is comparable to the atomic lattice spacing. Thus, the increases of characteristic temperatures reflect the change of phonon contributions.[23,26,30] For $Nb_5Ir_3O_{(1-\delta)}$, the $T_\mathrm{c}^\mathrm{onset}$, unit-cell volume, and lattice parameters $c/(10a)$ ratio are summarized in Fig. 5(b). With increasing $(1-\delta)$, $T_\mathrm{c}^\mathrm{onset}$ increases from ~ 9.4 K to ~ 10.15 K in Nb_5Ir_3O, the volume expands from ~ 272.89 mm^3 to ~ 273.05 mm^3, and $c/(10a)$ decreases from ~ 0.649 to ~ 0.647. More interestingly, $T_\mathrm{c}^\mathrm{onset}$ and the volume have similar linear dependence on $c/(10a)$. In Fig. 5(c), the relationship of $T_\mathrm{c}^\mathrm{onset}$ ($T_\mathrm{c}^\mathrm{zero}$) and T^p is also scaled. Both $T_\mathrm{c}^\mathrm{onset}$ and $T_\mathrm{c}^\mathrm{zero}$ decrease linearly with T^p. It is argued that T^p is proportional to the parameters closely correlated with θ_D, which implies that phonon contributions are different with pressures,[23,26] e.g., the weakness of phonon scattering and the reduced value of $\lambda_{\mathrm{e-p}}$.[5,15,17]

Finally, we discuss the evolution of superconditing transition temperature with the interstitial oxygen and pressures. As mentioned above, with increasing concentration of the interstitial oxygen, the volume expands and T_c enhances, which seems to contradict with pressure.[16] Under pressure, T_c correlates with the A value directly. As we know, A is proportional to the square of Sommerfeld coefficient, as an important measure of DOS at E_F. Therefore, the decrease of T_c mainly originates from the reduce of $N(E_\mathrm{F})$, which is consistent with the phonon-mediated behavior in Nb_5Ir_3O. Previous studies revealed that T_c will be higher if with larger $N(E_\mathrm{F})$.[15,17–19] It suggests that band filling effect is the main result of superconductivity. Or to say, high pressure and interstitial oxygen change the electronic structure and phonon spectrum in different ways. Several possible scenarios are proposed: the first case is that pressure broadens energy bands and results in the decrease of $N(E_\mathrm{F})$.[26] It is consistent with the fact that Nb_5Ir_3O is phonon-medicated SC. For $Nb_5Ir_3O_{(1-\delta)}$, the monotonic increase of $N(E_\mathrm{F})$ may account for higher T_c with increasing concentration of the interstitial oxygen. The second scenario is the weakness of $\lambda_{\mathrm{e-p}}$ under pressure, which can reduce T_c.[1,2] This is basically consistent with strong correlation characteristics of these SCs.[3,7,8,10] For $Nb_5Ir_3O_{(1-\delta)}$, considering the strong electronegativity of oxygen, the insertion of interstitial oxygen introduces Nb1–O ionic bonds, which may enhance the electron correlations and $\lambda_{\mathrm{e-p}}$. The third scenario is that Nb_5Ir_3O has an inter-band coupling considering its multi-band electronic structure, which usually appears in other multi-band SCs.[31,32] For $Nb_5Ir_3O_{(1-\delta)}$, the insertion of interstitial oxygen enhances this coupling and results in an enhancement of T_c, which is in good agreement with theoretical calculations. To understand the details, further studies on

band structures and phonon spectrum are also required.

In summary, we have investigated robust superconductivity and gap symmetry of Nb_5Ir_3O. Nb_5Ir_3O is found to be strongly coupled phonon-medicated SC with double s-waves. Phonon softening and low-lying phonon modes associated with the interstitial oxygen are critical to understand the evolution of T_c.

Acknowledgment

We thank S. Nagasaki and Dr. Gouchi for the technical assistance.

References

[1] Keppens V, Mandrus D, Sales B C, Chakoumakos B C, Dai P, Coldea R, Maple M B, Gajewski D A, Freeman E J and Bennington S 1998 *Nature* **395** 876
[2] Gunnarson O 1997 *Rev. Mod. Phys.* **69** 575
[3] Bauer E, Grysiv A, Chen X Q, *et al.* 2007 *Phys. Rev. Lett.* **99** 217001
[4] Hirai D, Ali M N and Cava R J 2013 *J. Phys. Soc. Jpn.* **82** 124701
[5] Hiroi Z, Yamaura J I and Hattori K 2012 *J. Phys. Soc. Jpn.* **81** 011012
[6] Testardi L R 1975 *Rev. Mod. Phys.* **47** 637
[7] Kudo K, Takasuga M, Okamoto Y, Hiroi Z and Nohara M 2012 *Phys. Rev. Lett.* **109** 097002
[8] Grosche F M, Yuan H Q, Cabrera W C, Paschen S, Langhammer C, Kromer F, Sparn G, Baenitz M, Grin Y and Steglich F 2001 *Phys. Rev. Lett.* **87** 247003
[9] Leithe J A, Schnelle W, Rosner H, Senthilkumaran N, Rabis A, Baenitz M, Gippius A, Morozova E, Mydosh J A and Grin Y 2003 *Phys. Rev. Lett.* **91** 037208
[10] Qi Y P, Lei H C, Guo J G, Shi W J, Yan B H, Felser C and Hosono H 2017 *J. Am. Chem. Soc.* **139** 8106
[11] Sales B C, Mandrus D and Williams R K 1996 *Science* **272** 1325
[12] Miyakawa M, Kim S W, Hirano M, Kohama Y, Kawaji H, Atake T, lkegami H, Kono K and Hosono H 2007 *J. Am. Chem. Soc.* **129** 7270
[13] Hosono H 2015 *Phil. Trans. R. Soc. A* **373** 20140450
[14] Crystal Structure Database at http://icsd.fiz-karlsruhe.de/accessed [201310-10]
[15] Lv B, Zhu X Y, Lorenz B, Wei F Y, Xue Y Y, Yin Z P, Kotliar G and Chu C W 2013 *Phys. Rev. B* **88** 134520
[16] Zhang Y Q, Wang B S, Xiao Z W, Lu Y F, Kamiya T, Uwatoko Y, Kageyana H and Hosono H 2017 *NPG Quan. Mater.* **2** 45
[17] Xie W W, Luo H X, Phelan B F and Cava R J 2015 *J. Mater. Chem. C* **3** 8235
[18] Li S, Liu X Y, An, V and Lv B 2018 *New J. Phys.* **20** 13009
[19] Bortolozo A D, Dos Santos C A M, Jardim R F, Ritter C, Devishvili A, Rotter M, Gandra F G and Machado A J S 2012 *J. App. Phys.* **111** 123912
[20] Koch C C and Scarbrough J O 1971 *Phys. Rev. B* **3** 742
[21] Horyń R, Folcik K L and Iliev N 1978 *J. Less Common Met.* **57** 69
[22] Mori N 2004 *High Press. Res.* **24** 225
[23] Golovashkin A I, Gudenko A V, Tskhovrebov A M, Zherikhina L N and Norton M L 1994 *Phys. C.* **235–240** 1481
[24] Gofryk K, Kaczorowski D, Plackowski T, Leithe J A and Grin Y 2005 *Phys. Rev. B* **72** 094409
[25] Kitawaki R and Terasaki I 2002 *J. Phys.: Condens. Matter* **14** 12495
[26] McMillan W L 1968 *Phys. Rev. B* **167** 331
[27] Bouquet F, Wang Y, Sheikin I, Plackowski T, Junod A, Lee S and Tajima S 2002 *Phys. Rev. Lett.* **89** 257001
[28] Bardeen J, Cooper L N and Schrieffer J R 1957 *Phys. Rev.* **108** 1175
[29] Johari G P *Chem. Phys.* **287** 273 Chumakov A I et al 2011 *Phys. Rev. Lett.* **106** 225501
[30] Cooper R A, Wang Y, Vignolle B, Lipscomne O J, Hayden S M, Tanabe Y, Adachi T, Koike Y, Nohara M, Takagi H, Proust C and Hussey N E 2009 *Science* **323** 603
[31] Subedi A, Zhang L J, Singh D J and Du M H 2008 *Phys. Rev. B* **78** 134514
[32] Forthaus M K, Sengupta K, Heyer O, Christensen N E, Svane A, Syassen K, Khomskii D I, Lorenz T and Abd-Elmeguid M M 2010 *Phys. Rev. Lett.* **105** 157001